Comprehensive genomic analysis of refractory multiple myeloma reveals a complex mutational landscape associated with drug resistance and novel therapeutic vulnerabilities

Nicola Giesen,[1,2*] Nagarajan Paramasivam,[3,4*] Umut H. Toprak,[3,5*] Daniel Huebschmann,[4,6,7,8*] Jing Xu,[1,2,9] Sebastian Uhrig,[4,9] Mehmet Samur,[10,11] Stella Bähr,[4] Martina Fröhlich,[4,9] Sadaf S. Mughal,[9] Elias K. Mai,[1] Anna Jauch,[12] Carsten Müller-Tidow,[1,13] Benedikt Brors,[8,9,13] Nikhil Munshi,[14] Hartmut Goldschmidt,[1,13] Niels Weinhold,[1#] Matthias Schlesner[3#] and Marc S. Raab[1,2#]

[1]Department of Internal Medicine V, Heidelberg University Hospital, Heidelberg, Germany; [2]Clinical Cooperation Unit Molecular Hematology/Oncology, Department of Internal Medicine V, Heidelberg University Hospital, and German Cancer Research Center (DKFZ), Heidelberg, Germany; [3]Bioinformatics and Omics Data Analytics, German Cancer Research Center (DKFZ), Heidelberg, Germany; [4]Computational Oncology, Molecular Diagnostics Program, National Center for Tumor Diseases (NCT) Heidelberg and German Cancer Research Center (DKFZ) Heidelberg, Germany; [5]Division of Neuroblastoma Genomics, German Cancer Research Center (DKFZ), Heidelberg, Germany; [6]Heidelberg Institute for Stem Cell Technology and Experimental Medicine (HI-STEM), Heidelberg, Germany; [7]Department of Pediatric Immunology, Hematology and Oncology, Heidelberg University Hospital, Heidelberg, Germany; [8]German Cancer Consortium (DKTK), Core Center Heidelberg, Germany; [9]Division of Applied Bioinformatics, German Cancer Research Center (DKFZ), Heidelberg, Germany; [10]Department of Data Sciences, Dana-Farber Cancer Institute, Boston, MA, USA; [11]Department of Biostatistics, Harvard TH Chan School of Public Health, Boston, MA, USA; [12]Institute for Human Genetics, Heidelberg University Hospital, Heidelberg, Germany; [13]National Center for Tumor Diseases (NCT), Heidelberg, Germany and [14]Jerome Lipper Multiple Myeloma Center, Department of Medical Oncology, Dana-Farber Cancer Institute, Boston, MA, USA

**NG, NP, UHT, and DH contributed equally as co-first authors.*
[#]NW, MS, and MSR contributed equally as co-senior authors.

Correspondence:

Marc S. Raab
m.raab@dkfz-heidelberg.de

Nicola Giesen
nicola.giesen@med.uni-heidelberg.de

Received: June 7, 2021.
Accepted: January 7, 2022.
Prepublished: January 20, 2022.
https://doi.org/10.3324/haematol.2021.279360

Supplementary Information

Supplementary Methods

Alignment of RRMM and NDMM

The raw reads were mapped to the human reference genome (build 37, version hs37d5), using BWA mem[1] (version 0.7.8, with parameter -T 0). A Phi X 174 contig (NC_001422.1) was added to the reference genome to remove the Phi X spike-in used during the sequencing. The mapped reads were sorted using SAMtools[2] (version 0.1.19), and lanes were merged and duplicate reads were marked using Sambamba[3] (version 0.5.9, with parameter -t 6 -l 9 --hash-table-size=2000000 --overflow-list-size=1000000 --io-buffer-size=64). Similar alignment workflow and parameters were applied to the raw reads from NDMM samples except that the BWA and Sambamba version were updated to 0.7.15 and 0.6.5 respectively.

To assess the effect of differing sequencing depths between the NDMM, RMM and RRMM samples on variant calling, subsampling of RRMM samples was performed using Sambamba (version 0.6.6, with parameters view -h -t 20 -s 0.5 -f bam --subsampling-seed=42) to achieve a 50% lower coverage which was comparable to the coverage of the set of NDMM (**suppl. Figure S1, S2**).

Small variant calling

SNVs and indels were called using in-house pipelines developed for the ICGC Pan-Cancer Analysis of Whole Genomes (PCAWG) project.[4] Briefly, SNVs were called in tumor samples using SAMtools mpileup (version 0.1.19, with parameters -REI -q 30 -ug) and bcftools view (with parameters -vcgN -p 2.0). We have disabled the Bayesian model in bcftools (by setting -p 2.0), which allows calling low variant allele frequency (VAF) variants. In the next step each of these variant positions were queried in the control sample using SAMtools mpileup (with parameters -ABRI -Q 0 -q 1). Variants were further annotated with Gencode[5] (version 19) and ANNOVAR[6]; 1000 genome variants, dbSNP variants and variant frequency from our local control were further annotated. Somatic variant classification and

confidence scores (with range 1 to 10) were added as described previously,[7] and variants with a score of 8 and above were considered as high confidence variants.

Indels were called together in control and tumor samples using Platypus[8] (version 0.8.1, with parameters -bufferSize = 100,000 -maxReads = 5,000,000) and gene definitions and databases were annotated similar to SNVs. As described previously,[9] somatic SNVs and indels present in ten or more samples in our local control database consisting of 280 WGS control samples from different cohorts, which were processed using the same pipelines, were considered as technical artifacts and were removed.

Further Combined Annotation Dependent Depletion (CADD) scores (version 1.3) were added to the variants.

Somatic small variants misclassified as germline variant due to contamination of normal control samples with tumor cell DNA were rescued using our in-house tool TiNDA, which uses the EM-algorithm implemented in Canopy[10] (version 1.2.0) to cluster variants based on VAFs. Clusters in which at least 85% of variants have a higher VAF in tumor compared to control and 85% of the variants have VAF below 0.45 in control and above 0.01 in tumor were considered as somatic clusters. Rescued variants with high confidence scores were merged with the remaining high confidence somatic variants.

Significance of subgroup differences (NDMM vs. RRMM) regarding mutational load were assessed by the Wilcoxon rank sum test.

The merged set of variants was used to identify driver genes using IntOGen[11] (version 3.0.5) with the parameters: --split-size 5000; with configuration: 'significance_threshold' as 0.1 for oncodrivefm, oncodriveclust and mutsig, 'samples_threshold' as 2 and 5 for oncodrivefm and oncodriveclst respectively. The identified driver genes were used to generate the oncoprint using ComplexHeatmap[12]. Significance of subgroup differences (NDMM vs. RRMM) regarding prevalences of gene mutations were assessed by Fisher's exact test.

Supervised analysis of mutational signatures

A supervised analysis of mutational signatures was performed with the R package YAPSA.[13] The function LCD_complex_cutoff() in YAPSA was used to compute a non-negative least square (NNLS) decomposition of the mutational catalogue with the 30 known signatures from COSMIC v2 (https://cancer.sanger.ac.uk/signatures/signatures_v2/). To unambiguously identify the used signature set we denominate these signatures as AC1–AC30 (as abbreviation for Alexandrov COSMIC). The MM1 signature which was recently linked to melphalan exposure was added.[14, 15] After a first NNLS decomposition, the computed exposures are compared to optimal signature-specific cutoffs in order to reduce false positive calls, and then only those signatures whose exposures are higher than these signature-specific cutoffs are kept for the analysis and fed into a second NNLS decomposition yielding the final exposures. YAPSA was also used for stratified analysis of mutational signatures in order to identify enrichment and depletion patterns. Breakpoint proximity was used as stratification axis with three strata: vicinity (distance to closest breakpoint < 100 kbp), intermediate (distance to closest breakpoint between 100 kbp and 1 Mbp), and background (distance to closest breakpoint > 1 Mbp). Significance of enrichment and depletion patterns as well as of subgroup differences (NDMM vs. RRMM) were assessed by the Kruskal Wallis test and if that revealed significance in more than two groups, Nemenyi tests were performed as post-hoc tests.

Identification of Kataegis clusters

As outlined previously,[16] we defined Kataegis-like clusters to be regions of increased SNV density with at least five SNVs with at most 1000 bp intermutational distance in one sample, similar to what has previously been defined as Kataegis.[17] We defined a Kataegis cluster to be recurrent if it was found in at least three samples, i.e., if in three samples Kataegis clusters were identified with a minimal region of overlap. Differences in the number of Kataegis clusters and in the prevalence of SNV location within and outside of Kataegis clusters in RRMM vs NDMM were assessed by Wilcoxon rank sum tests.

Structural variants

Structural variants (SVs) were detected using the DKFZ SOPHIA workflow version 2.0.2 available in https://github.com/DKFZ-ODCF/SophiaWorkflow with the source code of the SOPHIA algorithm available in https://bitbucket.org/utoprak/sophia/.[9, 16] SOPHIA is an SV detection algorithm incorporating discordant mate, split read and a background breakpoint database from 3417 blood samples of donors from published international and ongoing internal DKFZ projects. The data in the background breakpoint database is obtained from sequencing results across the 101bp Illumina Hiseq2000/2500 and 151bp Illumina Hiseq X-Ten technologies. The SV candidate detection is a process of split-read and discordant mate evidence collection across each breakpoint as precursors for a SV, and SV candidates (pairs of breakpoints) are filtered by a complex decision tree trained by expert assessment of orthogonal FISH data. Secondary translocations of the immunoglobulin loci were defined as secondary events with one of the breakpoints of the SV not further away than 2MB from the target breakpoint of a given primary immunoglobulin translocation (i.e. IG —PrimarySV—> PrimaryTarget —SecondarySV—>SecondaryTarget).

For the statistical comparison of NDMM and RRMM with respect to SV types, only SVs with discordant mate support were considered in order to exclude the influences of different WGS libraries used in the two projects executed in different sequencing centers. Discordance in terms of mate distance was defined as a mate distance more than 5*MedianInsertSize or mate read mapping to a different chromosome. This typically limits the scope of the comparison to SVs with sizes $\gtrsim$1000bps.

Comparison of SV counts between the RRMM and NDMM cohorts was made using the Kruskal-Wallis test. Chromoplexy and chromothripsis statuses were assigned by manual visual inspection of SV calls and copy-number profiles on CIRCOS plots.

Copy number variation detection

As described previously,[9, 16] copy number states were called and estimation of tumor purity and ploidy was performed using ACEseq (allele-specific copy number estimation from sequencing;

https://www.biorxiv.org/content/early/2017/10/29/210807). Structural variants called with SOPHIA were incorporated to improve genome segmentation. In cases where ACEseq provided multiple solutions for purity and ploidy, we manually selected the lowest ploidy solution which allowed to fit the majority of genomic segments to integer copy numbers and which also was consistent with the mutant allele frequency distribution of somatic SNVs. With regard to the TP53 containing region ACEseq plots were in addition inspected manually.

If at least 30% length of a chromosome arm or cytoband was affected by a CNV in a sample, then it was considered as chromosome arm-level or cytoband-level event for the sample. These sample level counts were used to find cytoband-level events that significantly differ between NDMM and RRMM cohorts. Significance of subgroup differences (NDMM vs. RRMM) were assessed by Fisher's exact test.

Calculation of measures of genomic instability

First, genome copy number data from ACEseq was smoothed to prevent artificially elevated genomic instability measures due to oversegmentation caused by technical noise. To this end, segments for which allele-specific copy numbers did not deviate by more than 0.3 from each other were merged. Furthermore, segments smaller than 3 Mb were merged to the more similar neighboring segment as previously described.[18] Additionally, in the same chromosome, when the segments in p-arm extend into the centromeric region and start within the centromeric region in the q-arm, the segments were merged. These smoothed and merged segments were used to calculate the homologous recombination deficiency (HRD) score[18] and the number of large-scale transitions (LST) as previously described.[19] Briefly, segments larger than 15 Mb that were less than a whole chromosome in length and corresponded to a loss of heterozygosity were counted for the HRD score. For the quantification of LSTs, breaks between segments of different total copy number were counted with the constraint that both segments had to be larger than 10 Mb but did not correspond to entire chromosome arms. In addition, the telomeric-allelic imbalance (TAI) score,[20] which corresponds to the number of chromosomal segments with minimum length of 11MB and allelic imbalance extending into the subtelomeric regions, was calculated using the smoothed ACEseq results.[21] Genomic instability was

quantified as the sum of HRD, LST, and TAI scores. Significance of subgroup differences (NDMM vs. RRMM) were assessed by the Wilcoxon rank sum test.

RNA sequencing

The paired-end reads were mapped to the STAR index generated reference genome (build 37, version hs37d5) using STAR[22] (version 2.5.2b). Genes' exons were defined by the GENCODE v19 gene models.[5] The gene expressions were quantified using featureCounts (Subread version 1.5.1). For differential gene expression analysis and detection of enhancer hijacking, raw read counts were normalized by a preliminary Counts Per Million (CPM) application where genes with less than 1 CPM were discarded from further analyses. Filtered gene read counts were normalized using the TMM method of the edgeR R package.[23, 24] TMM-normalized read counts were finalized by application of CPM and log2(x+1).

Gene fusions

Gene fusions were detected using Arriba version 1.0.0 (https://github.com/suhrig/arriba) as described previously.[25] To further enrich for high-confidence fusion predictions, events involving genes marked as putative by the gene model or events with fewer supporting reads than 1 % of the local coverage (<5 % for read-through fusions) were discarded.

References

1. Li H. Aligning sequence reads, clone sequences and assembly contigs with BWA-MEM. arXiv. 2013:1303.3997.

2. Li H, Handsaker B, Wysoker A, et al. The Sequence Alignment/Map format and SAMtools. Bioinformatics. 2009;25(16):2078-9.

3. Tarasov A, Vilella AJ, Cuppen E, Nijman IJ, Prins P. Sambamba: fast processing of NGS alignment formats. Bioinformatics. 2015;31(12):2032-4.

4. Consortium ITP-CAoWG. Pan-cancer analysis of whole genomes. Nature. 2020;578(7793):82-93.

5. Harrow J, Frankish A, Gonzalez JM, et al. GENCODE: the reference human genome annotation for The ENCODE Project. Genome Res. 2012;22(9):1760-74.

6. Wang K, Li M, Hakonarson H. ANNOVAR: functional annotation of genetic variants from high-throughput sequencing data. Nucleic acids research. 2010;38(16):e164.

7. Jones DT, Hutter B, Jager N, et al. Recurrent somatic alterations of FGFR1 and NTRK2 in pilocytic astrocytoma. Nature genetics. 2013;45(8):927-32.

8. Rimmer A, Phan H, Mathieson I, et al. Integrating mapping-, assembly- and haplotype-based approaches for calling variants in clinical sequencing applications. Nature genetics. 2014;46(8):912-8.

9. Paramasivam N, Hubschmann D, Toprak UH, et al. Mutational patterns and regulatory networks in epigenetic subgroups of meningioma. Acta Neuropathol. 2019;138(2):295-308.

10. Jiang Y, Qiu Y, Minn AJ, Zhang NR. Assessing intratumor heterogeneity and tracking longitudinal and spatial clonal evolutionary history by next-generation sequencing. Proceedings of the National Academy of Sciences of the United States of America. 2016;113(37):E5528-37.

11. Gonzalez-Perez A, Perez-Llamas C, Deu-Pons J, et al. IntOGen-mutations identifies cancer drivers across tumor types. Nat Methods. 2013;10(11):1081-2.

12. Gu Z, Eils R, Schlesner M. Complex heatmaps reveal patterns and correlations in multidimensional genomic data. Bioinformatics. 2016;32(18):2847-9.

13. Hubschmann D, Jopp-Saile L, Andresen C, et al. Analysis of mutational signatures with yet another package for signature analysis. Genes Chromosomes Cancer. 2021;60(5):314-31.

14. Rustad EH, Yellapantula V, Leongamornlert D, et al. Timing the initiation of multiple myeloma. Nature communications. 2020;11(1):1917.

15. Maura F, Degasperi A, Nadeu F, et al. A practical guide for mutational signature analysis in hematological malignancies. Nature communications. 2019;10(1):2969.

16. Lopez C, Kleinheinz K, Aukema SM, et al. Genomic and transcriptomic changes complement each other in the pathogenesis of sporadic Burkitt lymphoma. Nature communications. 2019;10(1):1459.

17. Alexandrov LB, Nik-Zainal S, Wedge DC, et al. Signatures of mutational processes in human cancer. Nature. 2013;500(7463):415-21.

18. Abkevich V, Timms KM, Hennessy BT, et al. Patterns of genomic loss of heterozygosity predict homologous recombination repair defects in epithelial ovarian cancer. British journal of cancer. 2012;107(10):1776-82.

19. Popova T, Manie E, Rieunier G, et al. Ploidy and large-scale genomic instability consistently identify basal-like breast carcinomas with BRCA1/2 inactivation. Cancer research. 2012;72(21):5454-62.

20. Birkbak NJ, Wang ZC, Kim JY, et al. Telomeric allelic imbalance indicates defective DNA repair and sensitivity to DNA-damaging agents. Cancer discovery. 2012;2(4):366-75.

21. Brok WDd, Schrader KA, Sun S, et al. Homologous Recombination Deficiency in Breast Cancer: A Clinical Review. JCO Precision Oncology. 2017(1):1-13.

22. Dobin A, Davis CA, Schlesinger F, et al. STAR: ultrafast universal RNA-seq aligner. Bioinformatics. 2013;29(1):15-21.

23. Robinson MD, Oshlack A. A scaling normalization method for differential expression analysis of RNA-seq data. Genome Biol. 2010;11(3):R25.

24. Robinson MD, McCarthy DJ, Smyth GK. edgeR: a Bioconductor package for differential expression analysis of digital gene expression data. Bioinformatics. 2010;26(1):139-40.

25. Heining C, Horak P, Uhrig S, et al. NRG1 Fusions in KRAS Wild-Type Pancreatic Cancer. Cancer discovery. 2018;8(9):1087-95.

Supplementary Figure legends

Suppl. Figure S1. RRMM original data vs RRMM subsampled data vs NDMM for graphs presented in main figure 1, analysis of Copy number variants in NDMM and RRMM patients, and Kataegis and SNV distribution in RRMM vs NDMM.

A. SV and SNV load per patient in RRMM original vs RRMM subsampled vs NDMM. SNV and SV counts are plotted for each patient showing a higher overall mutational load in RRMM, both the original data (orange) and the subsampled dataset (blue), vs NDMM (red). Each dot represents an individual patient. The example cases shown in main Figure 1, panels C and D, are annotated as RRMM_16 and RRMM_15, respectively.
B. Differences in SV types in RRMM original vs RRMM subsampled vs NDMM. Median and range of number of overall SVs per patient in RRMM, both original data (orange) and subsampled dataset (blue), vs NDMM (red) are shown as well as deletions (DEL), duplications (DUP), inversions (INV), and translocations (TRA).
C. Genome-wide small variant mutational load in RRMM original vs RRMM subsampled vs NDMM. The number of mutations per patients and length of genome in megabases (MB) is shown in RRMM, both original data (orange) and subsampled dataset (blue), vs NDMM (red).
D. Genomic instability scores in RRMM original vs RRMM subsampled vs NDMM. The unbiased sum of HRD, LST, and TAI scores is shown for RRMM, both original data (orange) and subsampled dataset (blue), vs NDMM (red) illustrating a higher genomic instability in RRMM.
E. Analysis of Copy number variants in NDMM and RRMM patients. Overview of somatic copy number aberrations (SCNAs) in NDMM vs RRMM patients. Orange indicates gain, blue indicates loss, red indicates loss of heterozygosity.
F. Recurrent regions of Kataegis in RRMM (blue) and NDMM (red) excluding the immunoglobulin loci. To compensate for differing sequencing depths in both cohorts, the RRMM dataset was subsampled for these analyses.

G. Kataegis and SNV distribution in RRMM vs NDMM. To compensate for differing sequencing depths in both cohorts, the RRMM dataset was subsampled for these analyses.

Suppl. Figure S2. RNA expression (A) and prediction of functional relevance by CADD score (B) of significant driver genes in RRMM.

A. Expression of small variants detected in significant driver genes in RRMM is indicated by variant allele frequency (VAF) in RNA sequencing with each dot representing an individual variant.
B. Prediction of functional relevance of small variants detected in significant driver genes in RRMM is indicated by Combined Annotation Dependent Depletion (CADD) score with each dot representing an individual variant. A CADD score > 20 indicates likely deleteriousness of the variant.

Suppl. Figure S3. Mutational frequency in gene groups/networks NDMM vs RRMM.

The prevalence of functional mutations in the following gene groups or networks in NDMM (red) vs RRMM (blue) is shown in the upper panel from left to right: genes associated with resistance to IMiDs, epigenetic modifiers, MAPK pathway, NFKB signaling, resistance to PIs, sensitivity to PARP inhibitors, NOTCH proteins, HECT E3 ubiquitin ligases, PI3K/AKT/MTOR signaling. In the lower panel statistical significance of mutation prevalence for each gene group are indicated. Details on composition of gene groups are given in supplemental Table S4.

Suppl. Figure S4. Mutations in gene group 'IMiD resistance' in RRMM.

Genes affected by SNVs or Indels in the gene group 'IMiD resistance' and their prevalence in the RRMM cohort are shown as well as copy number aberrations (CNAs) of chromosome arms 13q, 1q, 17p, 1p, presence or absence of hyperdiploid karyotype, and the genomic instability score.

Suppl. Figure S5. Mutations in gene group 'PI resistance' in RRMM.

Genes affected by SNVs or Indels in the gene group 'PI resistance' and their prevalence in the RRMM cohort are shown as well as copy number aberrations (CNAs) of chromosome arms 13q, 1q, 17p, 1p, presence or absence of hyperdiploid karyotype, and the genomic instability score.

Suppl. Figure S6. Mutations in gene group 'PARP inhibitor sensitivity' in RRMM.

Genes affected by SNVs or Indels in the gene group 'PAPR inhibitor sensitivity' and their prevalence in the RRMM cohort are shown as well as copy number aberrations (CNAs) of chromosome arms 13q, 1q, 17p, 1p, presence or absence of hyperdiploid karyotype, and the genomic instability score.

Suppl. Figure S7. Exposure to mutational signatures in RRMM original data vs RRMM subsampled data vs NDMM.

A. The absolute exposure to mutational signatures based on the Alexandrov COSMIC (AC) catalogue with the addition of the MM1 signature recently linked to melphalan exposure is shown for RRMM, both original data (orange) and subsampled dataset (blue), vs RMM (green) vs NDMM (red) patients. Most notable is an increased impact of signatures AC3 (light brown) and MM1 (black) in RRMM.
B. HRDetect scores in RRMM, both original data (orange) and subsampled dataset (blue), vs RMM (green) vs NDMM (red) patients.

Suppl. Figure S8. Highly complex IGL translocation in patient RRMM_34.

Translocations involving the immunoglobulin heavy chain (IGH) locus and the lambda light chain (IGL) are shown. Orange lines represent immunoglobulin locus translocations, purple lines represent secondary immunoglobulin locus related translocations, and names of partner genes are given. Secondary translocations of the immunoglobulin loci were defined as secondary events with one of the breakpoints of the SV not further away than 2MB from the target breakpoint of a given primary immunoglobulin translocation (i.e. IG —PrimarySV—> PrimaryTarget —SecondarySV—

>SecondaryTarget). To allow for better readability, relative size of chromosomes 11, 12, 14, and 22 are increased.

Suppl. Figure S9. *FAM46C* rearrangements in RRMM and expression analysis of target genes.

A. *FAM46C* rearrangements in RRMM. Green lines represent translocations, blue lines deletions, red lines duplications, and black lines inversions. Names of partner genes of interest are given, notable are *FAM46C*;*MYC* translocations. To allow for better readability, relative size of chromosome 1 is increased.
B. Gene expression profile of the *LMO4* gene across the RRMM cohort. The case with the putative enhancer hijacking of the *FAM46C* enhancer shows a markedly increased LMO4 expression.

Suppl. Figure S10. Gene expression of *MYC* (A), *CD40* (B), *H2AFJ* (C), *CXCR4* (D), *KMT2A* (E), and *CREBL2* (F) as opposed to expression of *MYCN*.

Expression of *MYC, CD40, H2AFJ*, *CXCR4, KMT2A,* and *CREBL2* for individual RRMM patients is shown by red lines, expression of *MYCN* by blue lines.

Supplementary Tables

Suppl. Table S1. Patient characteristics of RRMM cohort.

Suppl. Table S2. Detailed information on small variants in RRMM cohort.

Legend for table columns is as follows:

PID	
VAR_TYPE	SNVs or Indels
CHROM	
POS	
REF	
ALT	
VAR_SOURCE	Source of the somatic variant: Either from default somatic workflow or from TiNDA rescue
ANNOVAR_FUNCTION	Exonic or splicing
GENE	Gene name
EXONIC_CLASSIFICATION	Exonic protein sequence altering type
ANNOVAR_TRANSCRIPTS	Transcript information
Tumor_VAF	Tumor variant allele frequency (VAF)
Control_VAF	Control VAF
RNA_VAF	VAF in RNAseq data
ANNOTATION_RNA	Annotation tag about the expression status of the variant
CADD_PHRED	CADD (v1.3) score in Phred scale
gnomAD_MAF	GnomAD (v2.1) genome MAF
HYPER_DIPLOID	Hyper diploid sample classification
GENOMIC_INSTABILITY_SCORE	Genomic instability sample score
HRDetect	Genomic instability sample-level scores from HRDetect workflow
abs_AC3	Absolute AC3 mutational signature for the sample
norm_AC3	Normalized AC3 mutational signature for the sample

VAF: Variant allele frequency; MAF: Minor allele frequency; HRD: Homologous recombination deficiency; LST: Large-scale transition; TAI: Telomeric allelic imbalance; AC3: Alexandrov COSMIC signature 3

Suppl. Table S3. Analysis of mono- vs bi-allelic events.

Suppl. Table S4. Composition of gene groups and networks.

Suppl. Table S5. Detailed information on small variants in gene groups 'IMiD resistance', 'PI resistance', and 'PARP inhibitor sensitivity' in RRMM cohort.

Legend for table columns as described for suppl. Table S2.

Suppl. Table S6. Mutational signatures and asserted mutational mechanisms in RRMM cohort.

suppl. Figure S1

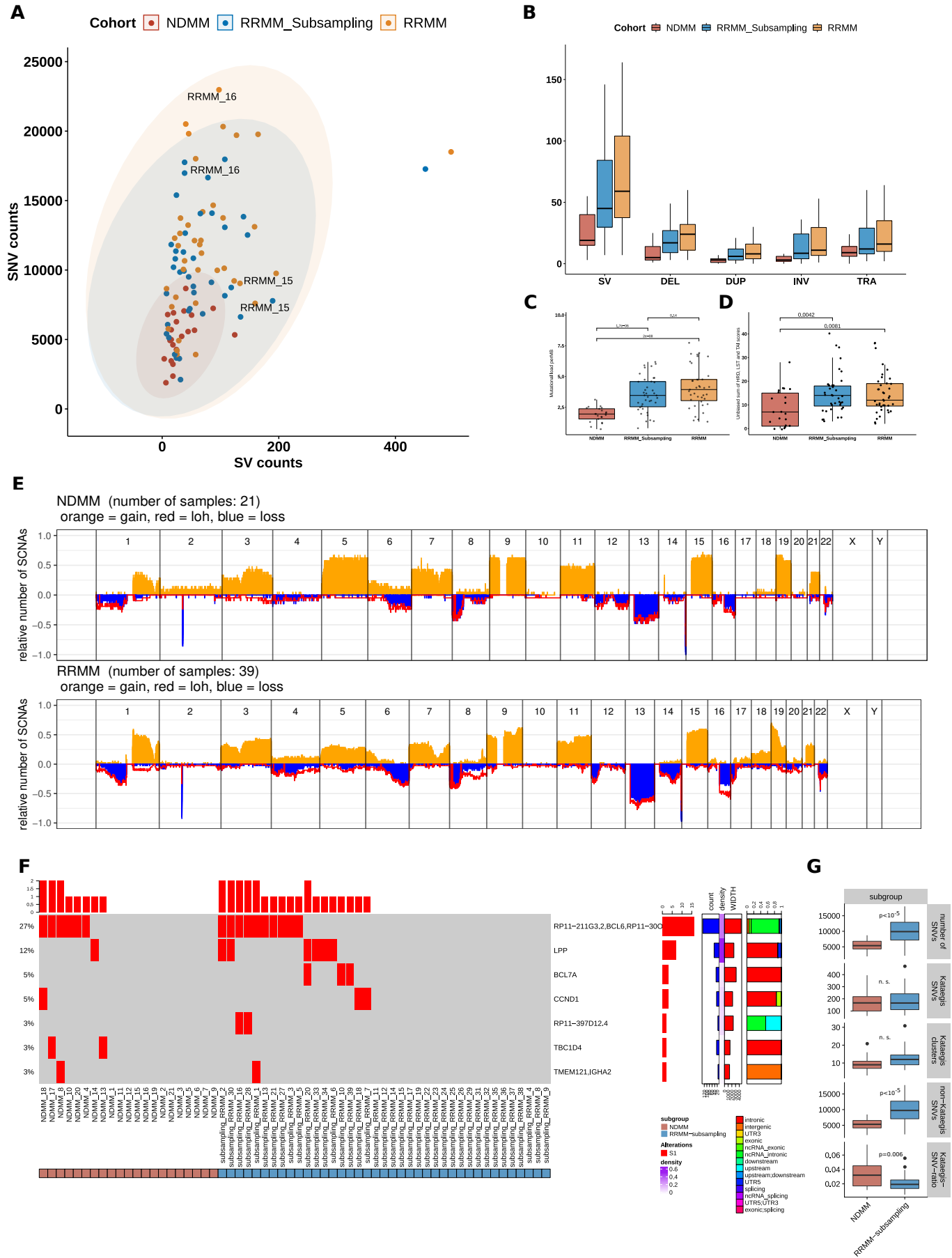

suppl. Figure S2

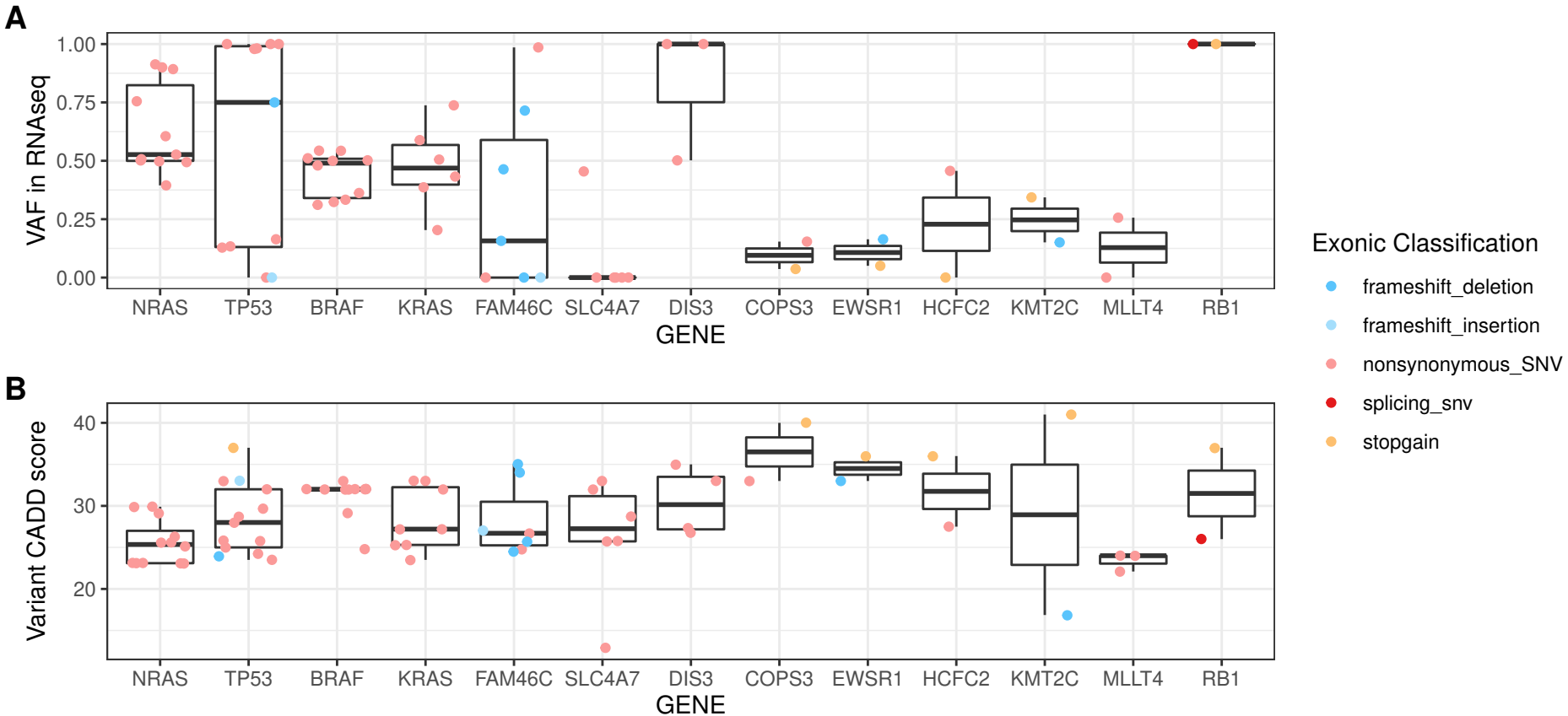

suppl. Figure S3

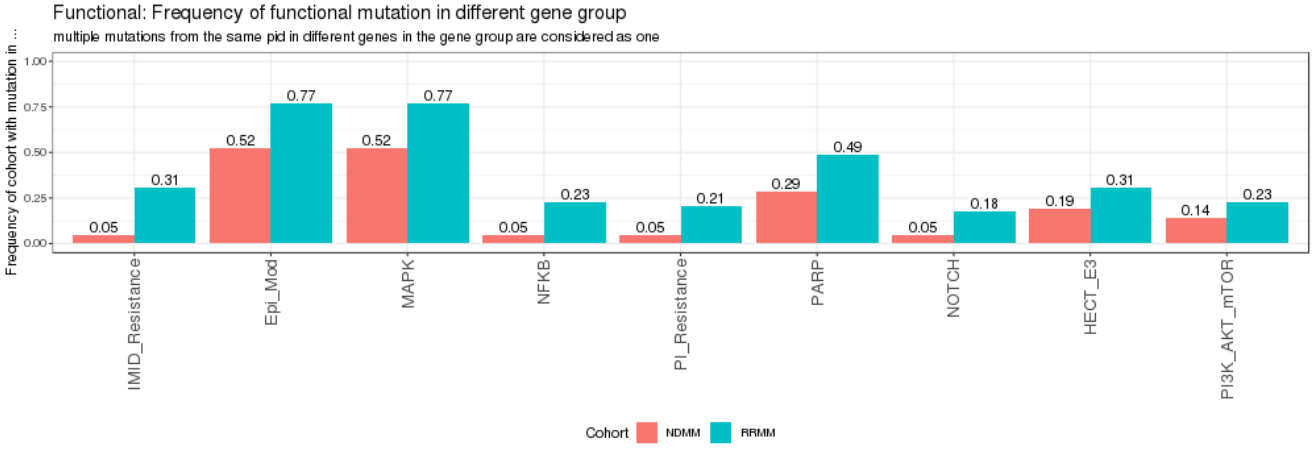

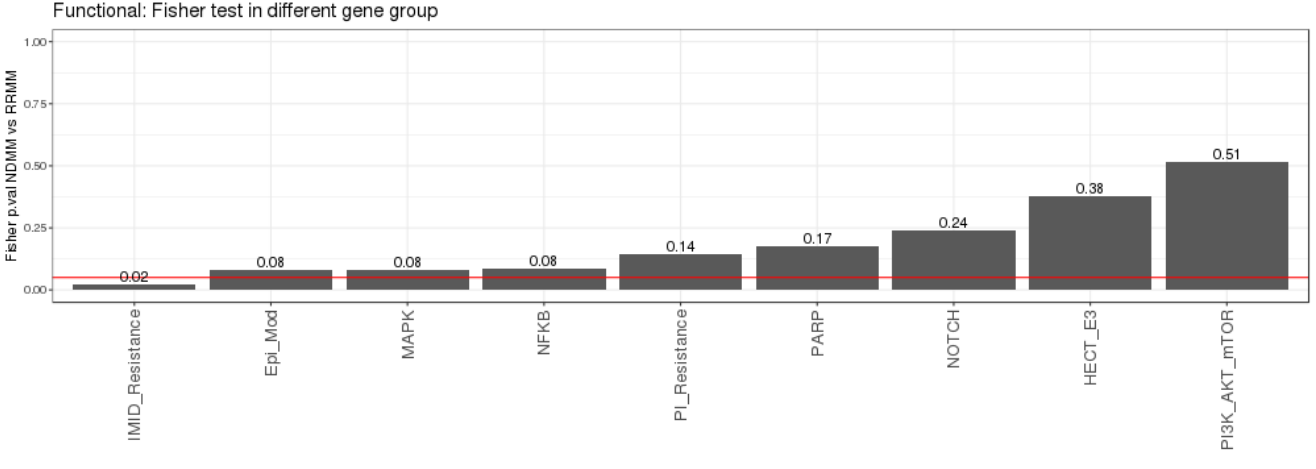

suppl. Figure S4

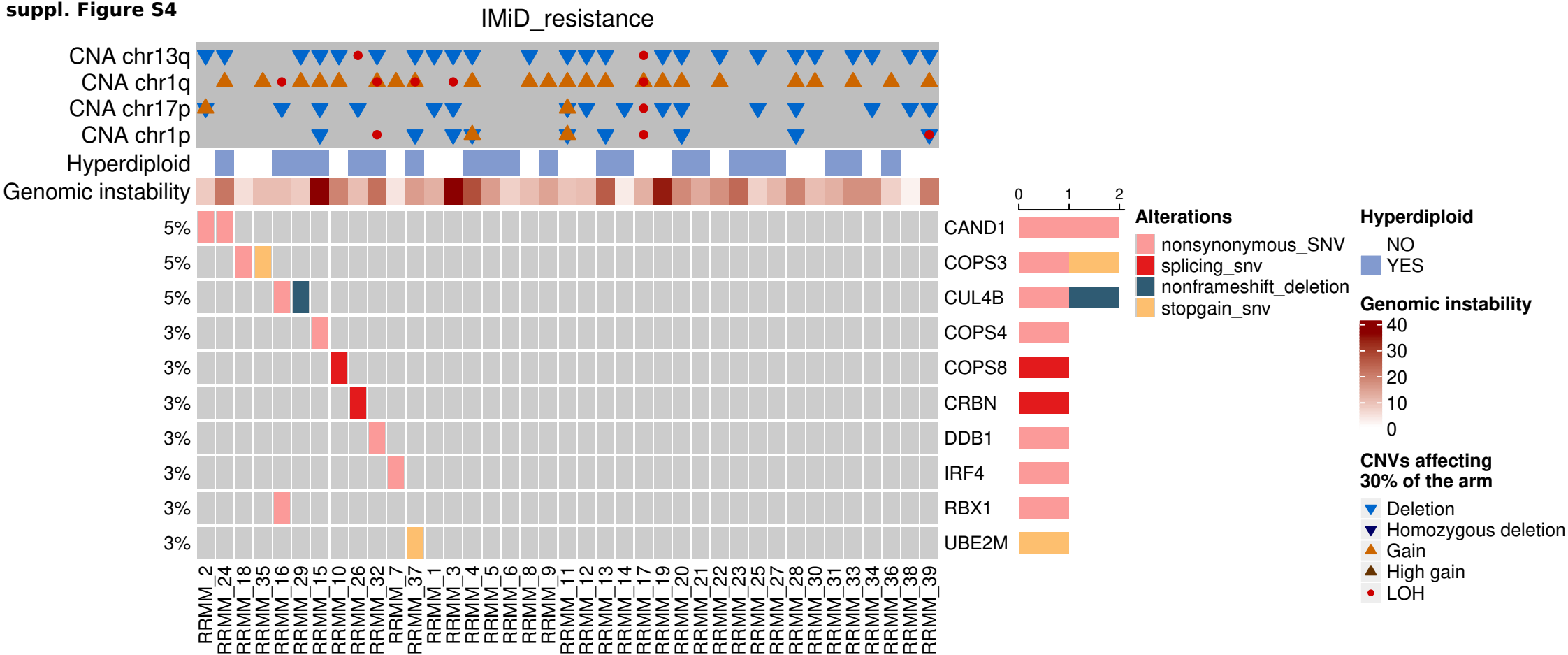

suppl. Figure S5

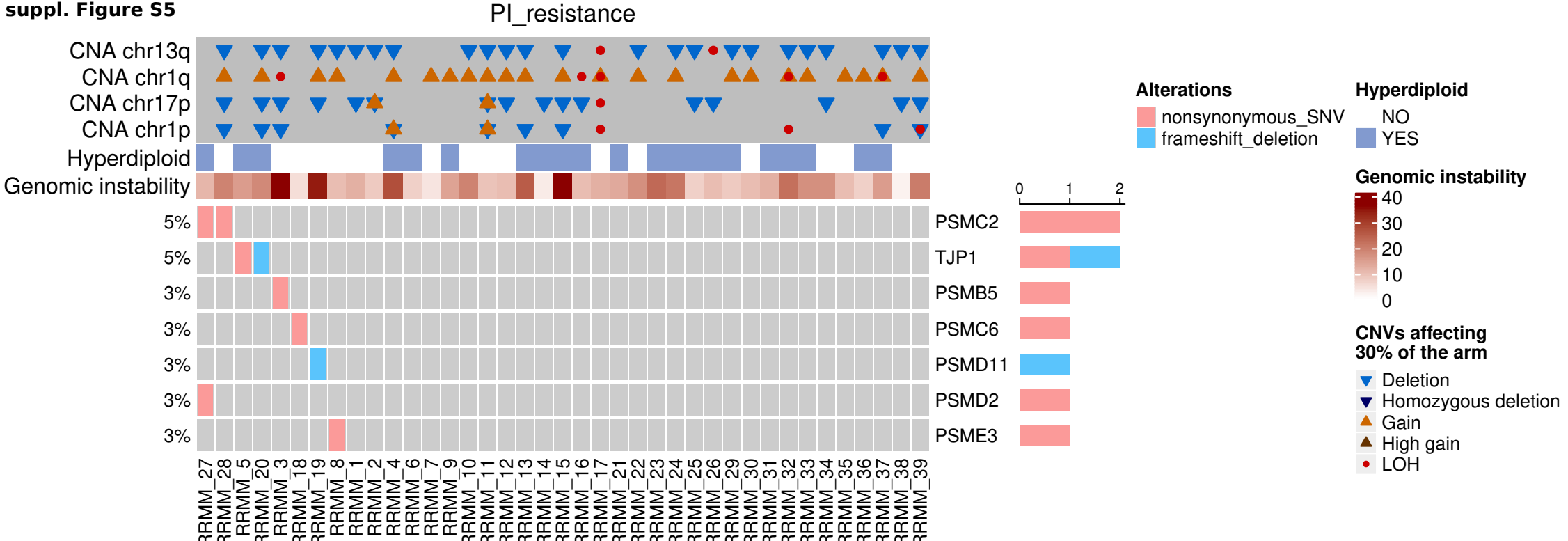

suppl. Figure S6

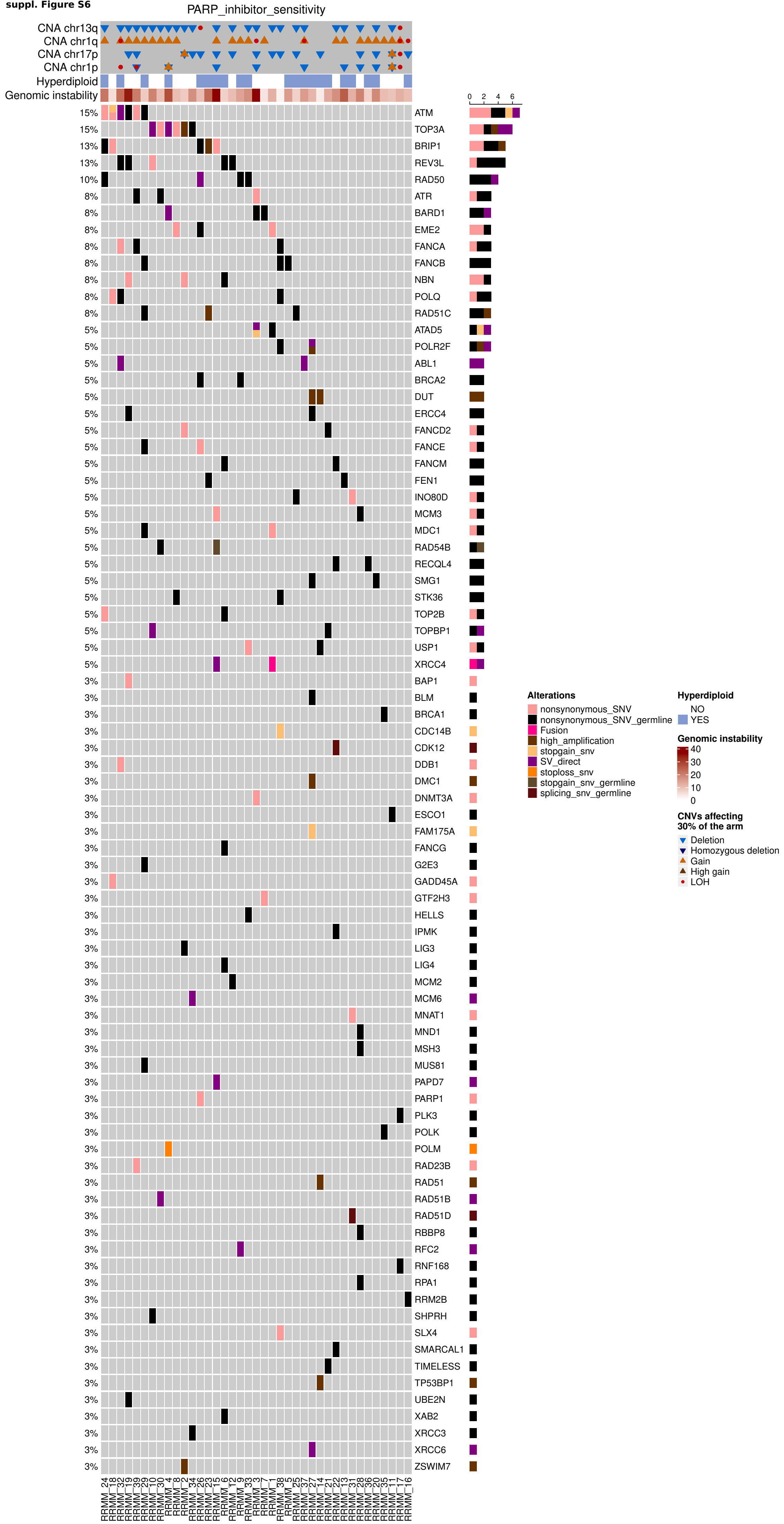

suppl. Figure S7

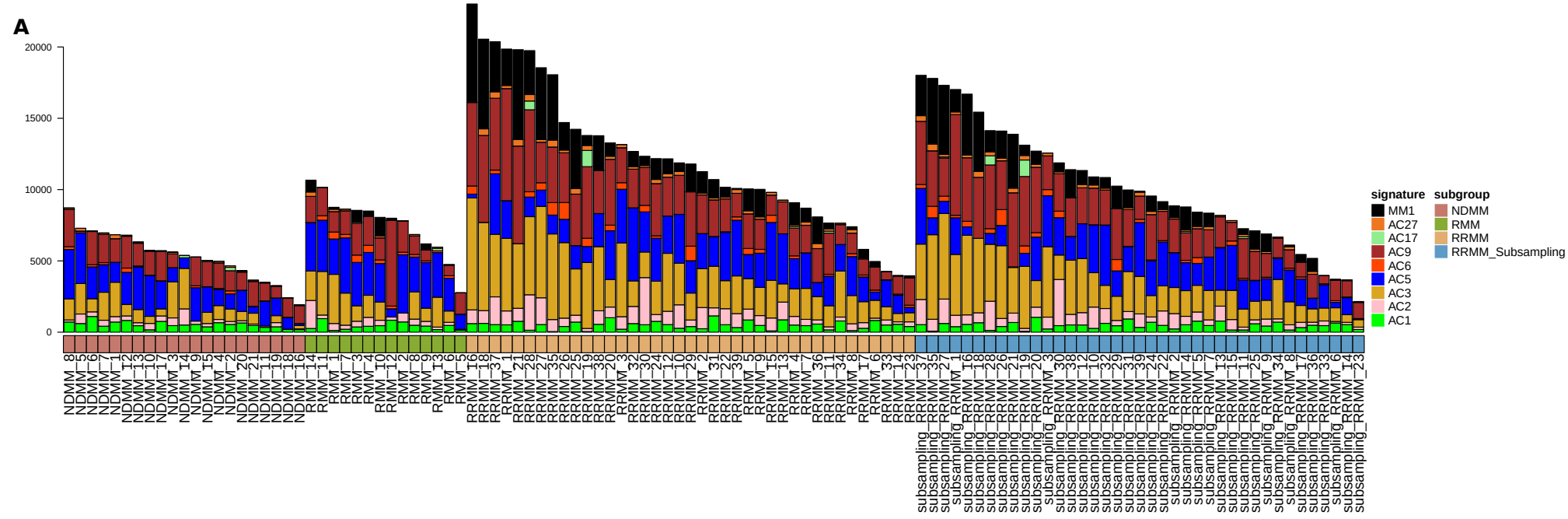

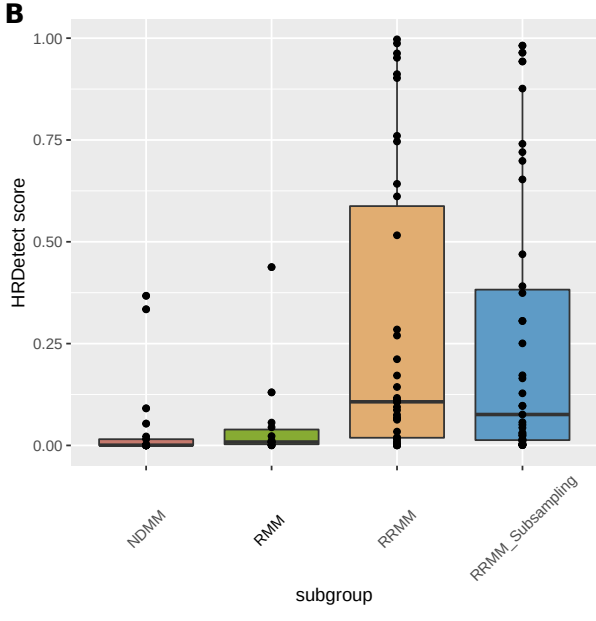

suppl. Figure S8

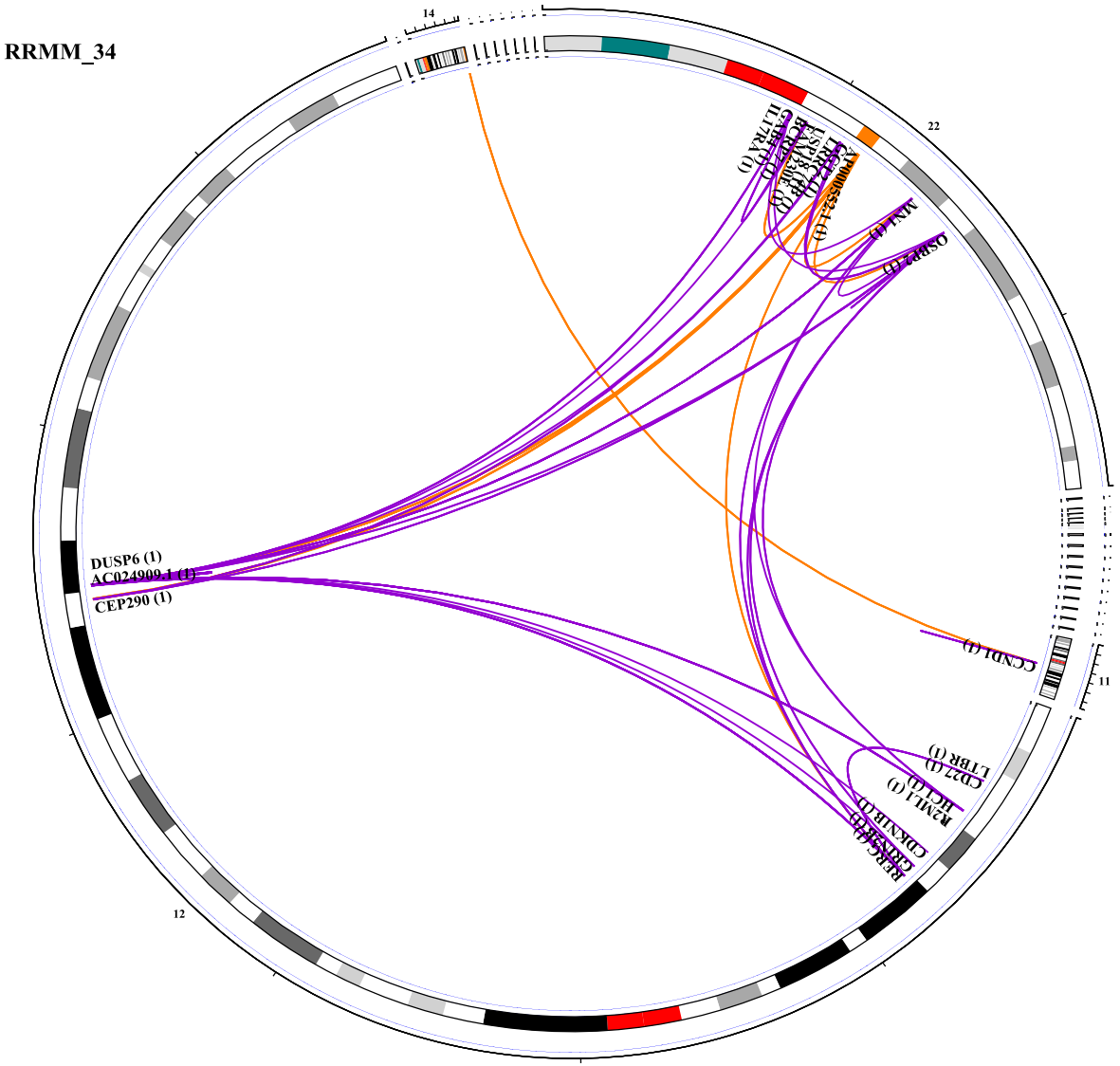

suppl. Figure S9

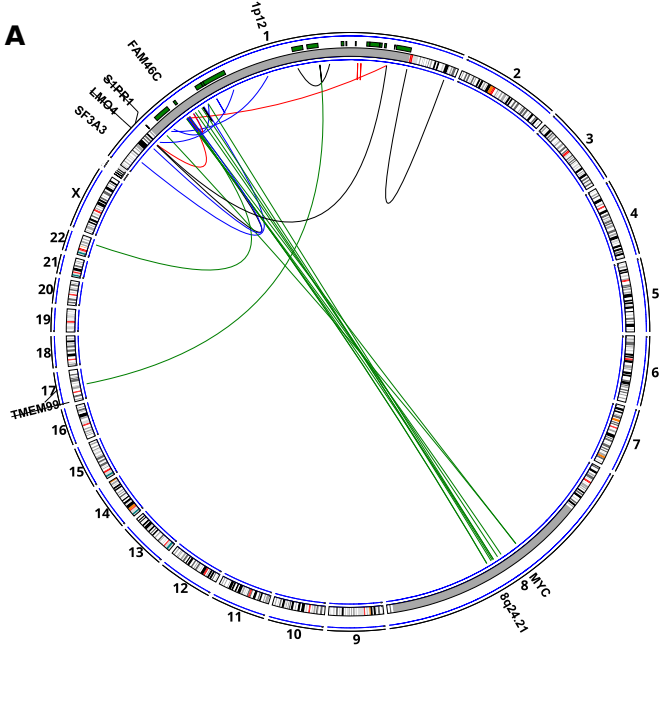

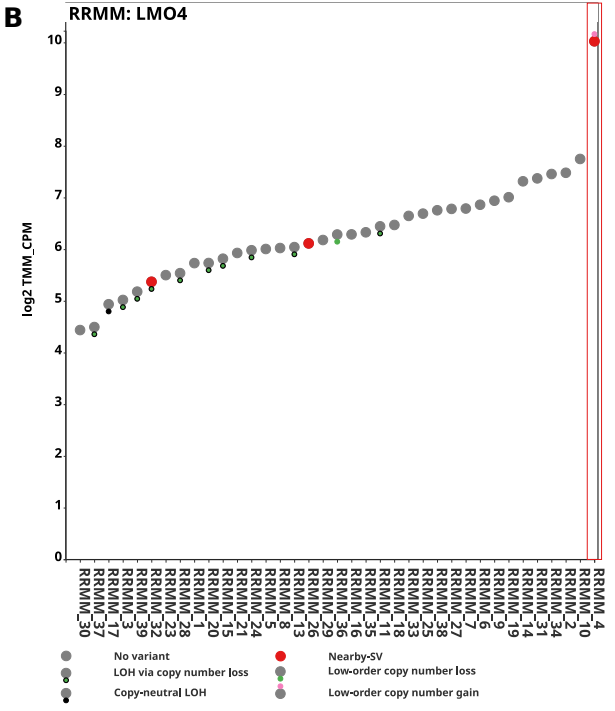

suppl. Figure S10

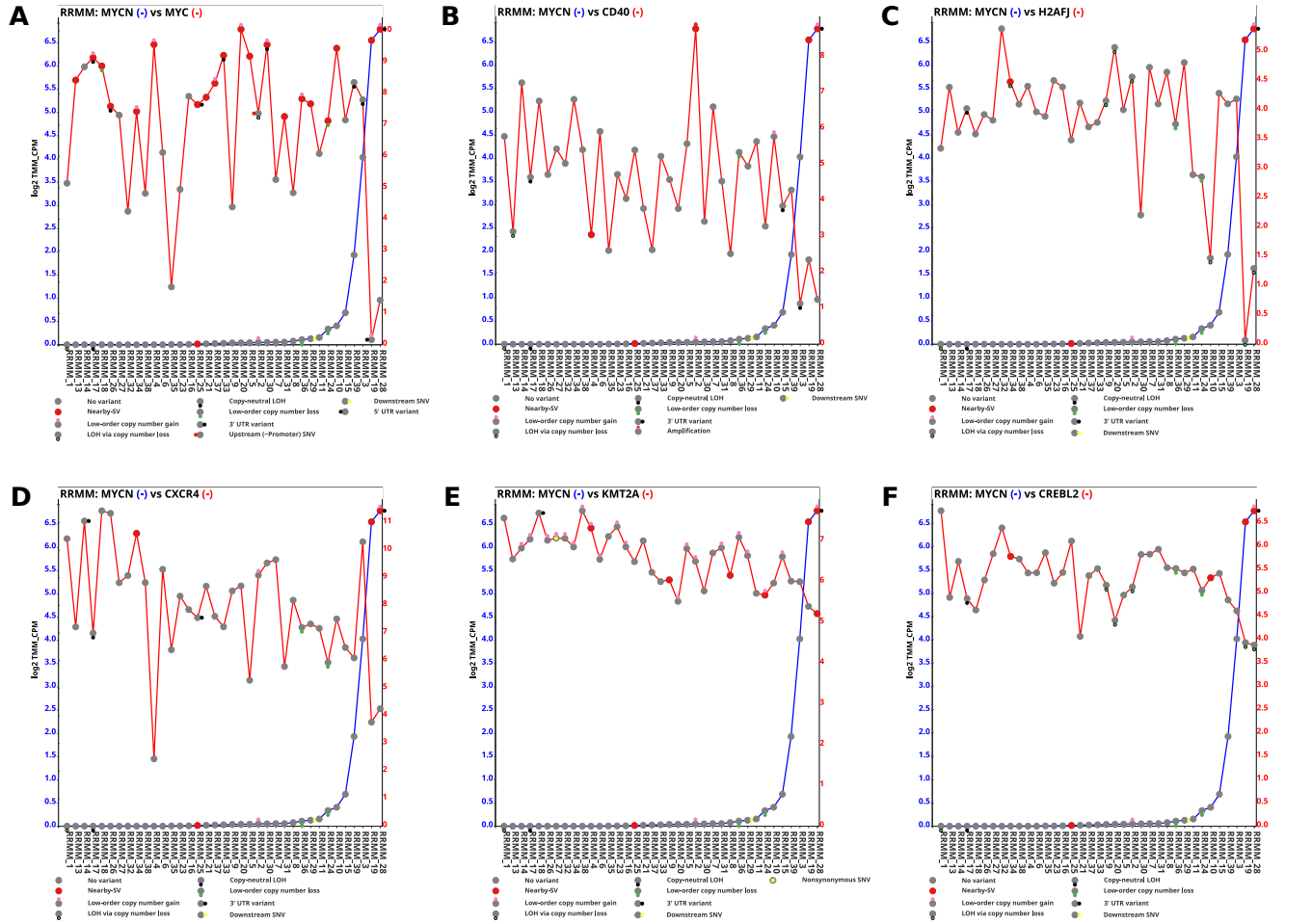

Suppl. Table S1: Patient characteristics of RRMM cohort.

ID	age (years)	sex	time from diagnosis (years)	MM type	ISS	hyperdiploid karyotype	high-risk cytogenetics at RRMM by FISH	#prior therapies	last therapy	prior IMID	prior PI	prior ASCT	refr to LEN	refr to POM	refr to BTZ	refr to CFZ	refr to CD38	part of cohort of Kortuem *et al.* (1)
RRMM_1	68	male	3,2	BJ lambda	2	no	del(17p)	6	CFZ-Dex	yes	yes	yes	yes	yes	yes	yes	no	no
RRMM_2	74	male	5,5	IgA kappa	2	no	del(17p), t(4;14)	4	CFZ-Dex	yes	yes	yes	yes	no	yes	yes	no	yes
RRMM_3	40	male	1,5	IgG kappa	2	no	del(17p)	2	LEN-Cy-Dex	yes	yes	yes	yes	no	yes	no	no	no
RRMM_4	65	female	3,2	IgG kappa	3	yes	no	5	CFZ-Dex	yes	yes	yes	yes	yes	yes	yes	no	no
RRMM_5	70	female	6,2	IgG lambda	2	yes	no	4	POM-Cy-Dex	yes	yes	yes	yes	yes	no	yes	no	no
RRMM_6	56	male	10,1	IgG kappa	1	yes	no	4	POM-Dex	yes	yes	yes	yes	yes	no	no	no	no
RRMM_7	59	male	7,3	IgG kappa	1	no	no	5	CFZ-LEN-Dex	yes	yes	yes	yes	no	yes	yes	no	no
RRMM_8	78	male	4,7	BJ lambda	3	no	>3 copies 1q21	6	CFZ-Dex	yes	yes	no	yes	yes	yes	yes	no	no
RRMM_9	67	male	16,0	IgA kappa	na	yes	no	8	POM-Dex	yes	yes	yes	yes	yes	yes	yes	no	yes
RRMM_10	73	female	4,1	IgG kappa	2	no	del(17p), >3 copies 1q21, t(4;14)	8	CFZ-Dex	yes	yes	yes	yes	yes	yes	yes	no	no
RRMM_11	71	male	3,9	IgA lambda	3	no	>3 copies 1q21, t(4;14)	5	POM-Dex	yes	yes	yes	yes	yes	yes	no	no	yes
RRMM_12	76	female	7,4	IgG kappa	na	no	>3 copies 1q21	9	POM-Dex	yes	yes	no	no	yes	yes	no	no	no
RRMM_13	78	female	2,2	IgG kappa	2	yes	no	3	CD38-POM-Dex	yes	yes	no	yes	yes	yes	no	yes	no
RRMM_14	63	female	1,8	IgA lambda	2	yes	del(17p)	3	CFZ-Cy-Dex	yes	yes	yes	yes	no	no	yes	no	no
RRMM_15	49	male	1,3	IgG kappa	2	yes	del(17p), >3 copies 1q21	4	POM-Dex	yes	yes	yes	yes	yes	yes	no	no	no
RRMM_16	75	male	11,1	IgG kappa	na	yes	del(17p)	8	CFZ-Dex	yes	yes	yes	yes	yes	yes	yes	no	no
RRMM_17	55	female	1,4	IgG kappa	1	no	del(17p)	3	POM-Dex	yes	yes	yes	yes	yes	yes	no	no	no
RRMM_18	67	female	9,5	IgG lambda	1	no	no	6	CFZ-LEN-Dex	yes	yes	yes	yes	yes	yes	yes	no	no
RRMM_19	66	male	3,9	IgA lambda	3	no	del(17p), t(4;14)	4	SLAMF7-POM-Dex	yes	yes	yes	yes	yes	yes	yes	no	no
RRMM_20	65	female	4,2	IgG kappa	1	yes	del(17p), >3 copies 1q21	3	POM-Dex	yes	yes	yes	no	yes	yes	no	no	yes
RRMM_21	64	female	12,8	IgG kappa	na	yes	no	6	CFZ-LEN-Dex	yes	yes	yes	yes	no	no	yes	no	no
RRMM_22	69	male	4,2	IgG lambda	2	no	del(17p), t(4;14)	11	Ruxolitinib	yes	yes	yes	yes	yes	yes	yes	no	no
RRMM_23	77	male	12,9	IgA lambda	3	yes	no	7	POM-Dex	yes	yes	yes	yes	yes	no	no	no	no
RRMM_24	68	male	5,9	IgG kappa	3	yes	>3 copies 1q21	5	POM-Dex	yes	yes	yes	yes	yes	yes	no	no	no
RRMM_25	53	female	8,6	IgG kappa	2	yes	del(17p)	8	POM-Dex	yes	yes	yes	yes	yes	yes	yes	no	yes
RRMM_26	54	male	2,1	IgG kappa	3	yes	no	3	POM-Dex	yes	yes	yes	yes	yes	no	no	no	yes
RRMM_27	62	female	4,4	IgG kappa	1	yes	no	4	POM-Dex	yes	yes	yes	no	yes	yes	no	no	no
RRMM_28	47	male	1,9	BJ lambda	na	no	del(17p), >3 copies 1q21, t(4;14)	3	CFZ-LEN-Dex	yes	yes	yes	yes	no	yes	yes	no	no
RRMM_29	67	female	6,8	IgG kappa	na	yes	no	9	CFZ-Dex	yes	yes	yes	yes	yes	yes	yes	no	no
RRMM_30	51	male	4,4	BJ lambda	na	no	>3 copies 1q21	8	CFZ-Dex	yes	yes	yes	yes	yes	no	yes	no	no
RRMM_31	53	male	6,8	IgG kappa	2	yes	no	5	CFZ-Dex	yes	yes	yes	yes	no	no	yes	no	yes
RRMM_32	85	female	13,2	BJ lambda	1	yes	no	13	CFZ-Cy-Dex	yes	yes	no	yes	yes	yes	yes	no	yes
RRMM_33	48	female	1,7	IgG lambda	na	yes	no	5	CFZ-Dex	yes	yes	yes	yes	yes	yes	yes	no	yes
RRMM_34	63	female	3,4	IgG lambda	1	no	del(17p)	3	POM-Dex	yes	yes	yes	yes	yes	yes	yes	no	no
RRMM_35	42	female	7,0	IgG lambda	1	no	no	13	CD38-LEN-Dex	yes	yes	yes	yes	yes	yes	yes	yes	no
RRMM_36	38	male	2,4	IgA lambda	3	yes	no	5	BTZ-THA-Dex-PACE	yes	yes	yes	yes	no	yes	yes	no	no
RRMM_37	70	male	5,0	IgA kappa	1	yes	no	5	CFZ-Dex	yes	yes	yes	yes	no	no	yes	no	no
RRMM_38	60	male	9,6	IgG kappa	1	no	del(17p)	4	LEN-Dex	yes	yes	yes	yes	no	yes	no	no	no
RRMM_39	64	female	3,3	BJ kappa	1	no	del(17p)	5	POM-Dex	yes	yes	no	yes	yes	yes	no	yes	no

abbreviations: MM - multiple myeloma; BJ - bence jones; ISS - international staging system; na - not available; CFZ - carfilzomib; Dex - dexamethasone; LEN - lenalidomide; Cy - cyclophosphamide; POM - pomalidomide; CD38 - anti-CD38 monoclonal antibody; SLAMF7 - anti-SLAMF7 monoclonal antibody; BTZ - bortezomib; THA - thalidomide; PACE - cisplatin, adriamycin, cyclophosphamide, etoposide; IMID - immunomodulatory agent; PI - proteasome inhibitor; ASCT - autologous stem cell transplantation; refr - refractory. (1) Kortüm et al. Blood 2016, Targeted sequencing of refractory myeloma reveals a high incidence of mutations in CRBN and Ras pathway genes.

Suppl. Table S3: Analysis of mono- vs bi-allelic events.

ID	CDKN2C	FAM46C	ASXL2	BIRC2	RB1	PCDH17	TRAF3	CYLD	WWOX	TP53	NF1	IGLL5	SNX29	NBAS	MMRN1
RRMM_1	wildtype	wildtype	bi-allelic	wildtype	mono-allelic	mono-allelic	wildtype	wildtype	wildtype	mono-allelic	mono-allelic	mono-allelic	wildtype	bi-allelic	wildtype
RRMM_2	wildtype	wildtype	wildtype	wildtype	mono-allelic	mono-allelic	mono-allelic	mono-allelic	mono-allelic	bi-allelic	wildtype	wildtype	wildtype	wildtype	wildtype
RRMM_3	mono-allelic	mono-allelic	wildtype	wildtype	mono-allelic	mono-allelic	bi-allelic	wildtype	wildtype	bi-allelic	bi-allelic	mono-allelic	wildtype	wildtype	mono-allelic
RRMM_4	wildtype	mono-allelic	wildtype	wildtype	bi-allelic	mono-allelic	wildtype	mono-allelic	mono-allelic	wildtype	wildtype	wildtype	wildtype	wildtype	bi-allelic
RRMM_5	wildtype	bi-allelic	wildtype	wildtype	wildtype	wildtype	wildtype	mono-allelic	mono-allelic	wildtype	wildtype	mono-allelic	wildtype	wildtype	wildtype
RRMM_6	wildtype	mono-allelic	wildtype	wildtype	wildtype	wildtype	wildtype	wildtype	wildtype	wildtype	wildtype	wildtype	wildtype	wildtype	mono-allelic
RRMM_7	wildtype	wildtype	wildtype	wildtype	mono-allelic	mono-allelic	wildtype	wildtype	wildtype	wildtype	wildtype	wildtype	wildtype	wildtype	wildtype
RRMM_8	wildtype	wildtype	wildtype	bi-allelic	mono-allelic	mono-allelic	wildtype	wildtype	wildtype	wildtype	wildtype	mono-allelic	wildtype	wildtype	wildtype
RRMM_9	wildtype	wildtype	wildtype	mono-allelic	wildtype	wildtype	wildtype	wildtype	wildtype	wildtype	wildtype	mono-allelic	wildtype	wildtype	wildtype
RRMM_10	wildtype	mono-allelic	wildtype	wildtype	bi-allelic	bi-allelic	wildtype	mono-allelic	wildtype	bi-allelic	wildtype	mono-allelic	wildtype	wildtype	wildtype
RRMM_11	mono-allelic	mono-allelic	wildtype	wildtype	mono-allelic	mono-allelic	bi-allelic	wildtype	wildtype	mono-allelic	wildtype	bi-allelic	wildtype	wildtype	wildtype
RRMM_12	wildtype	wildtype	wildtype	mono-allelic	bi-allelic	mono-allelic	wildtype	wildtype	wildtype	mono-allelic	wildtype	wildtype	wildtype	wildtype	wildtype
RRMM_13	wildtype	mono-allelic	wildtype	wildtype	mono-allelic	bi-allelic	wildtype	wildtype	wildtype	wildtype	mono-allelic	bi-allelic	wildtype	wildtype	wildtype
RRMM_14	wildtype	wildtype	wildtype	wildtype	bi-allelic	wildtype	wildtype	mono-allelic	mono-allelic	bi-allelic	wildtype	bi-allelic	wildtype	wildtype	wildtype
RRMM_15	bi-allelic	mono-allelic	wildtype	wildtype	mono-allelic	mono-allelic	wildtype	mono-allelic	mono-allelic	bi-allelic	wildtype	wildtype	bi-allelic	wildtype	mono-allelic
RRMM_16	wildtype	wildtype	wildtype	wildtype	wildtype	wildtype	wildtype	wildtype	wildtype	mono-allelic	mono-allelic	wildtype	wildtype	wildtype	wildtype
RRMM_17	wildtype	wildtype	wildtype	wildtype	wildtype	wildtype	wildtype	wildtype	wildtype	bi-allelic	wildtype	bi-allelic	wildtype	wildtype	wildtype
RRMM_18	wildtype	wildtype	wildtype	wildtype	wildtype	wildtype	wildtype	bi-allelic	mono-allelic	wildtype	wildtype	mono-allelic	wildtype	wildtype	wildtype
RRMM_19	wildtype	mono-allelic	mono-allelic	wildtype	mono-allelic	mono-allelic	mono-allelic	mono-allelic	mono-allelic	bi-allelic	wildtype	bi-allelic	wildtype	bi-allelic	wildtype
RRMM_20	mono-allelic	mono-allelic	wildtype	wildtype	mono-allelic	mono-allelic	wildtype	wildtype	wildtype	mono-allelic	wildtype	mono-allelic	wildtype	wildtype	wildtype
RRMM_21	wildtype	wildtype	wildtype	wildtype	wildtype	wildtype	wildtype	wildtype	wildtype	mono-allelic	wildtype	mono-allelic	mono-allelic	wildtype	wildtype
RRMM_22	wildtype	wildtype	wildtype	wildtype	mono-allelic	mono-allelic	wildtype	wildtype	wildtype	wildtype	wildtype	bi-allelic	wildtype	wildtype	wildtype
RRMM_23	wildtype	mono-allelic	wildtype	wildtype	mono-allelic	wildtype	wildtype	wildtype	wildtype	wildtype	wildtype	wildtype	wildtype	wildtype	wildtype
RRMM_24	wildtype	mono-allelic	wildtype	wildtype	mono-allelic	mono-allelic	wildtype	mono-allelic	mono-allelic	wildtype	wildtype	wildtype	wildtype	wildtype	mono-allelic
RRMM_25	wildtype	wildtype	wildtype	wildtype	bi-allelic	mono-allelic	wildtype	mono-allelic	mono-allelic	mono-allelic	wildtype	wildtype	wildtype	wildtype	mono-allelic
RRMM_26	wildtype	wildtype	wildtype	wildtype	wildtype	wildtype	wildtype	bi-allelic	wildtype	mono-allelic	wildtype	wildtype	wildtype	wildtype	wildtype
RRMM_27	wildtype	wildtype	wildtype	wildtype	wildtype	wildtype	wildtype	wildtype	wildtype	wildtype	wildtype	bi-allelic	wildtype	wildtype	wildtype
RRMM_28	wildtype	mono-allelic	wildtype	wildtype	bi-allelic	mono-allelic	wildtype	wildtype	wildtype	mono-allelic	wildtype	bi-allelic	wildtype	mono-allelic	wildtype
RRMM_29	wildtype	mono-allelic	wildtype	wildtype	mono-allelic	mono-allelic	wildtype	wildtype	wildtype	wildtype	wildtype	wildtype	wildtype	wildtype	wildtype
RRMM_30	wildtype	bi-allelic	wildtype	wildtype	mono-allelic	mono-allelic	bi-allelic	wildtype	mono-allelic	wildtype	wildtype	bi-allelic	wildtype	wildtype	wildtype
RRMM_31	wildtype	wildtype	wildtype	wildtype	wildtype	wildtype	wildtype	wildtype	wildtype	wildtype	wildtype	wildtype	wildtype	wildtype	wildtype
RRMM_32	wildtype	wildtype	wildtype	wildtype	mono-allelic	mono-allelic	wildtype	bi-allelic	mono-allelic	wildtype	wildtype	bi-allelic	wildtype	wildtype	wildtype
RRMM_33	wildtype	mono-allelic	wildtype	wildtype	mono-allelic	mono-allelic	bi-allelic	wildtype	wildtype	wildtype	wildtype	bi-allelic	wildtype	wildtype	wildtype
RRMM_34	wildtype	wildtype	wildtype	wildtype	mono-allelic	mono-allelic	wildtype	wildtype	mono-allelic	bi-allelic	mono-allelic	wildtype	wildtype	wildtype	wildtype
RRMM_35	wildtype	wildtype	wildtype	wildtype	wildtype	wildtype	wildtype	bi-allelic	wildtype	wildtype	wildtype	bi-allelic	wildtype	wildtype	wildtype
RRMM_36	wildtype	wildtype	wildtype	wildtype	wildtype	wildtype	wildtype	mono-allelic	mono-allelic	wildtype	wildtype	bi-allelic	wildtype	wildtype	wildtype
RRMM_37	mono-allelic	mono-allelic	wildtype	wildtype	bi-allelic	mono-allelic	bi-allelic	mono-allelic	mono-allelic	wildtype	wildtype	wildtype	wildtype	wildtype	wildtype
RRMM_38	wildtype	wildtype	wildtype	wildtype	mono-allelic	bi-allelic	wildtype	wildtype	wildtype	mono-allelic	wildtype	wildtype	wildtype	wildtype	wildtype
RRMM_39	mono-allelic	mono-allelic	wildtype	wildtype	mono-allelic	mono-allelic	bi-allelic	wildtype	wildtype	mono-allelic	wildtype	wildtype	wildtype	wildtype	wildtype

Suppl. Table S4: Composition of gene groups and networks.

resistance to PIs	resistance to IMiDs	PARP inhibitor sensitivity				MAPK pathway	NFKB signaling
PSMC1	CRBN	ABL1	GEN1	PRMT6	USP7	ARAF	REL
PSMC2	IZKF1	ATAD5	GIYD1	PSMC3IP	WRN	BRAF	RELA
PSMC3	IZKF3	ATM	GIYD2	PTEN	XAB2	RAF1	RELB
PSMC4	IRF4	ATR	GTF2H3	RAD21	XRCC2	MAP2K1	NFKB1
PSMC5	CUL4A	AURORA	HELLS	RAD23B	XRCC3	MAP2K2	NFKB2
PSMC6	CUL4B	BAP1	HUS1	RAD50	XRCC4	MAPK1	IKBKB
TJP1	DDB1	BARD1	INIP	RAD51	XRCC6	MAPK3	CHUK
PSMB9	RBX1	BLM	INO80D	RAD51B	ZSWIM7	HRAS	IKBKG
PSMB8	COPS1	BRCA1	IPMK	RAD51C		KRAS	NFKBIA
PSMB5	COPS2	BRCA2	KAT5	RAD51D		NRAS	TRADD
ERN1	COPS3	BRCC3	LIG3	RAD52		SOS1	RIPK1
XBP1	COPS4	BRIP1	LIG4	RAD54B		SOS2	TRAF2
PSMA1	COPS5	CDC14B	MAD2L2	RAD54L		NF1	TRAF5
PSMA2	COPS6	CDK12	MAPK12	RBBP8		GRB2	MAP3K14
PSMA3	COPS7	CDK5	MCM2	RECQL4		RASA1	BIRC2
PSMA4	COPS8	CDK7	MCM3	REV3L		RASA2	BIRC3
PSMA5	CAND1	CHEK1	MCM6	RFC2		PTPN11	TRAF3
PSMA6	UBE2M	CHEK2	MDC1	RNF168		RASGRF1	TRAF1
PSMA7	UBE2D3	DDB1	miR-103	RPA1		RASGRF2	TRAF6
PSMA8	UBE2G1	DMC1	miR-107	RRM1		RASGRP1	TAK1
PSMB1		DNASE1L2	miR-222	RRM2B		RASGRP2	NFKBIB
PSMB2		DNMT3A	miR-506	SHFM1		RASGRP3	NFKBIE
PSMB3		DUT	miR-9	SHPRH		RASGRP4	IRAK1
PSMB4		EME1	MMS22L	SLX4		RASAL1	TRAF7
PSMB6		EME2	MNAT1	SMARCA2		RASAL2	RIPK2
PSMB7		ERCC1	MND1	SMARCA5		RASA4	RIPK3
PSMB10		ERCC4	MRE11A	SMARCAL1		RASA3	
PSMB11		ERCC8	MSH3	SMC3			
PSMD1		ESCO1	MUM1	SMG1			
PSMD2		ESCO2	MUS81	SPO11			
PSMD3		EWSR1-FLI1	NAMPT	SSRP1			
PSMD4		FAAP20	NAP1L1	STK36			
PSMD7		FAAP24	NBN	SUMO1			
PSMD8		FAM175A	ORC1L	TEX11			
PSMD11		FANCA	ORC5L	TIMELESS			
PSMD12		FANCB	PALB2	TMPRSS2-ERG			
PSMD13		FANCC	PAPD7	TOP2B			
PSMD14		FANCD2	PARP1	TOP3A			
PSME1		FANCE	PLK3	TOPBP1			
PSME2		FANCF	PNKP	TP53BP1			
PSME3		FANCG	POLB	TTDN1			
PSME4		FANCI	POLD3	UBA1			
PSMF1		FANCL	POLH	UBE2A			
SHFM1		FANCM	POLK	UBE2N			
ADRM1		FEN1	POLM	UNG			
		G2E3	POLQ	USP1			
		GADD45A	POLR2F	USP10			

epigenetic modifiers							
HIST1H1A	H2BFM	PHF2	HDAC5	ARID1B	CTCF		
HIST1H1B	H2BFWT	PHF8	HDAC6	ARID2	MBD1		
HIST1H1C	HIST1H3A	ASH1L	HDAC7	ARID3A	MBD2		
HIST1H1D	HIST1H3B	CARM1	HDAC8	ARID3B	MBD3		
HIST1H1E	HIST1H3C	DOT1L	HDAC9	ARID3C	MBD4		
HIST1H1T	HIST1H3D	EED	SIRT1	ARID4A	MBD5		
H1FOO	HIST1H3E	EHMT1	SIRT2	ARID4B	MBD6		
H1FNT	HIST1H3F	EHMT2	SIRT3	ARID5A	MECP2		
H1F0	HIST1H3G	EZH1	SIRT4	ARID5B	RAG2		
H1FX	HIST1H3H	EZH2	SIRT5	ASXL1	TDG		
HIST1H2AA	HIST1H3I	MEN1	SIRT6	ATRX	TP53BP1		
HIST1H2AB	HIST1H3J	NSD1	SIRT7	BRD7			
HIST1H2AC	HIST2H3D	PRDM2	ZBTB33	CHD1			
HIST1H2AD	HIST3H3	PRMT1	BRPF1	CHD2			
HIST1H2AE	H3F3A	PRMT2	CLOCK	CHD3			
HIST1H2AG	H3F3B	PRMT5	CREBBP	CHD4			
HIST1H2AH	H3F3C	PRMT6	ELP3	CHD5			
HIST1H2AJ	HIST1H4A	PRMT7	EP300	CHD6			
HIST1H2AK	HIST1H4B	SETD1A	EP400	CHD8			
HIST1H2AL	HIST1H4C	SETD1B	GNAT1	CHD9			
HIST1H2AM	HIST1H4D	SETD2	GNAT2	DPF1			
HIST2H2AB	HIST1H4E	SETD3	GNAT3	DPF2			
HIST2H2AC	HIST1H4F	SETD7	GTF3C4	INO80			
HIST3H2A	HIST1H4G	SETD8	HAT1	KLF1			
H2AFB3	HIST1H4H	SETDB1	KAT2A	MLF1IP			
H2AFJ	HIST1H4I	SETDB2	KAT2B	PBRM1			
H2AFV	HIST1H4J	SETMAR	KAT5	PHF10			
H2AFX	HIST1H4K	SMYD1	KAT6A	RBBP4			
H2AFY	HIST1H4L	SMYD2	KAT6B	SET			
H2AFY2	HIST4H4	SMYD3	KAT7	SMARCA1			
H2AFZ	KDM1A	SUV39H1	KAT8	SMARCA2			
HIST1H2BA	KDM1B	SUV39H2	MORF4L1	SMARCA4			
HIST1H2BB	KDM2A	SUV420H1	NCOA1	SMARCA5			
HIST1H2BC	KDM2B	SUV420H2	NCOA2	SMARCAD1			
HIST1H2BD	KDM3A	SUZ12	NCOA3	SMARCAL1			
HIST1H2BE	KDM3B	WHSC1	TAF1	SMARCB1			
HIST1H2BF	KDM4A	WHSC1L1	TAF1L	SMARCC1			
HIST1H2BG	KDM4B	KMT2A	TAF3	SMARCC2			
HIST1H2BH	KDM4C	KMT2D	DNMT1	SMARCD1			
HIST1H2BI	KDM4D	KMT2C	DNMT3A	SMARCD2			
HIST1H2BJ	KDM5A	KMT2B	DNMT3B	SMARCD3			
HIST1H2BK	KDM5B	KMT2E	IDH1	SMARCE1			
HIST1H2BL	KDM5C	BAZ2A	IDH2	SRCAP			
HIST1H2BM	KDM5D	HDAC1	TET1	BPTF			
HIST1H2BN	KDM6A	HDAC10	TET2	BRD2			
HIST1H2BO	KDM6B	HDAC11	TET3	BRD4			
HIST2H2BE	KDM7A	HDAC2	ACTL6A	BRD8			
HIST2H2BF	KDM8	HDAC3	ACTL6B	CBX5			
HIST3H2BB	UTY	HDAC4	ARID1A	CBX7			

PI3K/AKT/ MTOR pathway	NOTCH receptors	HECT E3 ligases	references
PIK3CA	NOTCH1	NEDD4	Barrio et al. Leukemia 2018, Spectrum and functional validation of PSMB5 mutations in multiple myeloma.
PIK3CB	NOTCH2	NEDD4L	
PIK3CD	NOTCH3	SMURF1	Cargnello et al. Microbiol Mol Biol Rev. 2011, Activation and Function of the MAPKs and Their Substrates, the MAPK-Activated Protein Kinases.
PIK3R1	NOTCH4	SMURF2	
PIK3R2		ITCH	Hayden et al. Cell 2008, Shared principles in NF-kappaB signaling.
PIK3R3		WWP1	Karin et al. Nature 2006, Nuclear factor-kappaB in cancer development and progression.
PIK3R5		WWP2	
PIK3R6		HECW1	Karnoub et al. Nat Rev Mol Cell Biol. 2008, Ras oncogenes: split personalities.
PIK3CG		HECW2	
PTEN		HERC1	Krönke et al. Science 2014, Lenalidomide Causes Selective Degradation of IKZF1 and IKZF3 in Multiple Myeloma Cells
AKT1		HERC2	
AKT2		HERC3	Laplante et al. Cell 2012, mTOR Signaling in Growth Control and Disease.
AKT3		HERC4	Leung-Hagesteijn et al. Cancer Cell 2013, Xbp1s-Negative Tumor B Cells and Pre-Plasmablasts Mediate Therapeutic Proteasome Inhibitor Resistance in Multiple Myeloma
PDK1		HERC5	
MTOR		HERC6	
RICTOR		UBE3A	Lord et al. Nat Rev Cancer 2016, BRCAness revisited.
TCL1A		UBR5	Nowell et al. Nat Rev Cancer 2017, Notch as a tumour suppressor.
TCL1B		HACE1	Pawlyn et al. Clin Cancer Res 2016, The Spectrum and Clinical Impact of Epigenetic Modifier Mutations in Myeloma.
PHLPP1		HUWE1	
PHLPP2		HECT2D	Rotin et al. Nat Rev Mol Cell Biol 2009, Physiological functions of the HECT family of ubiquitin ligases.
TSC1		HECTD4	
TSC2		TRIP12	Shaw et al. Nature 2006, Ras, PI(3)K and mTOR signalling controls tumour cell growth.
RHEB		G2E3	
RPTOR		HECTD1	Shi et al. Mol Cancer Ther 2017, CRISPR Genome-Wide Screening Identifies Dependence on the Proteasome Subunit PSMC6 for Bortezomib Sensitivity in Multiple Myeloma.
EIF4EBP1		UBE3B	
EIF4E		UBE3C	
RPS6KB1		AREL1	Sievers et al. Blood 2018, Genome-wide screen identifies cullin-RING ligase machinery required for lenalidomide-dependent CRL4CRBN activity
EIF4B		HECTD3	
RPS6			
MLST8			Sun et al. Cell Res. 2011, Non-canonical NF-κB signaling pathway.
AKT1S1			Tanaka et al. 2009, Proc Jpn Acad Ser B Phys Biol Sci:The proteasome: overview of structure and functions.
DEPTOR			
TTI1			Thorpe et al. Nat Rev Cancer 2015, PI3K in cancer: divergent roles of isoforms, modes of activation and therapeutic targeting.
TELO2			
MAPKAP1			Vigil et al. Nat Rev Cancer 2010, Ras superfamily GEFs and GAPs: validated and tractable targets for cancer therapy?
PRR5			
PRR5L			Zhang et al. Cancer Cell 2016, Tight Junction Protein 1 Modulates Proteasome Capacity and Proteasome Inhibitor Sensitivity in Multiple Myeloma via EGFR/JAK1/STAT3 Signaling.

Suppl. Table S6. Mutational signatures and asserted mutational mechanisms in RRMM cohort.

Name	Correspondence in COSMIC v2	colour	Mutational mechanism
AC1	SBS1	green	Clock-like; spontaneous deamination
AC2	SBS2	pink	APOBEC
AC3	SBS3	gold	Homologous recombination repair deficiency
AC5	SBS5	blue	Clock-like, mechanism unknown
AC6	SBS6	orange	Mismatch repair deficiency
AC9	SBS9	brown	Polymerase η
AC17	SBS17	lightgreen	mechanism unknown
AC27	SBS27	chocolate	mechanism unknown
MM1	-	black	melphalan